An Analytic Model of the Agulhas Current as a Western Boundary Current with Linearly Varying Viscosity

DAVID J. WEBB

Southampton Oceanography Centre, Southampton, United Kingdom

(Manuscript received 23 February 1998, in final form 27 July 1998)

ABSTRACT

A recent current profile across the Agulhas Current shows a region of strong current shear near the continental slope and a relatively gentle exponential decay of the current offshore. If the standard Munk solution is used to fit the current profile, it can account for only 76% of the variance in the data. In an attempt to provide a better fit, the problem of a western boundary current with a linearly increasing viscosity coefficient is solved analytically. It is found that the new solution can explain 97.3% of the variance in the data. The addition of a constant viscosity inshore layer produces a further significant improvement, the final solution explaining 98.2% of the total variance.

1. Introduction

Recently Bryden (Bryden 1995; Beal and Bryden 1997) used an Acoustic Doppler Current Profiler (ADCP) to measure the velocity structure of the Agulhas Current. The section along which measurements were made ran perpendicular to the coast starting from a point approximately 200 km southwest of Durban. It was similar to the section sampled earlier by Toole and Warren (1993) and was chosen because the current is closest to the coast at this point and exhibits minimal meandering (Grundlingh 1983).

The data from 237 m, the greatest depth for which continuous data were obtained, are plotted in Fig. 1. The data from shallower depths have the same general behavior but exhibit extra variability, possibly due to the surface Ekman layer.

The results show that the Agulhas Current has a narrow maximum about 13 km from the continental slope, after which the velocity decays approximately exponentially offshore. The exponential decay is similar to that observed in a Stommel-type[1] western boundary current dominated by bottom friction. However, bottom friction is unlikely to be involved because the depth is too great (1400 m at the current maximum and increasing rapidly offshore) and there is additional evidence for a countercurrent at 1000 m. Bottom friction also cannot explain the current maximum.

A current maximum can be produced by a Munk-type western boundary current theory using constant horizontal viscosity. However, as shown in Fig. 1, if the Munk solution is fitted to the whole of the data using least squares, then the best fit has a scale length (38.4 km), which is too large to successfully reproduce the narrow peak of the current. As a result, only 76% of the total variance of the data is explained. At 31.5°S the scale length corresponds to a horizontal viscosity of 1101 $m^2\ s^{-1}$.

If the Munk solution is fitted to data near the peak, (9–43 km from the coast), then the scale length is reduced to 14.8 km and the viscosity to 63 $m^2\ s^{-1}$. This second solution certainly matches the peak of the current but, when compared to the data, the solution decays too rapidly offshore.

Other hypotheses may also be considered. MacCready and Rhines (1993) have proposed that the bottom boundary layer can be important in boundary currents, but, as with the Stommel theory, the depth of water and the presence of a deep countercurrent (Beal and Bryden 1997) mean that this approach is unlikely to be applicable to the present data. Other possibilities include internal wave drag and a shear stress that does not depend on the local velocity gradient.

It is also possible that what we are seeing in the data is the effect of the nearby coastline on the turbulent structure of the flow (Ellison 1956; Landau and Lifshitz 1987). In this case, simple eddy viscosity ideas are still valid, but we need to allow for the average scale of the

[1] Note that Stommel's theory was developed to explain the westward intensification of boundary currents, not their detailed structure.

Corresponding author address: Dr. David J. Webb, James Rennell Division, Southampton Oceanography Centre, Empress Dock, Southampton SO14 3ZH, United Kingdom.
E-mail: David.Webb@soc.soton.ac.uk

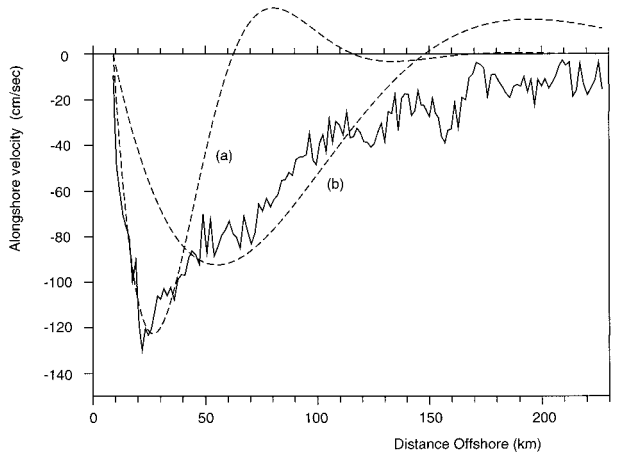

FIG. 1. Solid curve is the ADCP current data at a depth of 237 m for a section crossing the Agulhas Current, at an angle of 130° relative to true north near 31.5°S. At this depth the edge of the continental slope is 8.6 km from the coast. Dotted curves are the best-fit Munk solutions to (a) data between 9 and 43 km, (b) data between 9 and 227 km.

eddies to increase in size away from the coastline, resulting in increased viscosity. The above estimates of viscosity are certainly consistent with such behavior.

The present paper considers this approach in more detail, concentrating on cases where the viscosity is either constant or increases linearly with distance from the coast. Unfortunately, we start without a theory for the structure of a western boundary current when the viscosity is varying. As a result the present paper is in two parts. The first, sections 2–5, develops the analytic theory of western boundary currents for the case where the viscosity increases linearly away from the coast. It also derives a number of results applicable to any theory based on boundary currents in which the alongshore pressure gradient is balanced by a horizontal shear stress.

The second part of the paper then uses the analytic solutions to obtain best fits to the Agulhas Current data of Bryden (1995). It is shown that a linearly increasing viscosity gives a much better fit than the standard Munk solution. If this is matched to a constant viscosity region near the shore, then a further improvement can be obtained.

2. A western boundary current with horizontal viscosity

In a steady Munk-type western boundary current, along a north–south boundary, the dominant terms in the eastward and northward momentum equations are

$$-fv = -\frac{1}{\rho_0}\frac{\partial p}{\partial x},$$

$$0 = -\frac{1}{\rho_0}\frac{\partial p}{\partial y} + \frac{\partial}{\partial x}\left(A_h\frac{\partial}{\partial x}\right)v. \tag{1}$$

Here x and y are the east–west and north–south coordinates, positive to the east and north respectively; f is the Coriolis parameter, equal to $2\Omega\sin\phi$, where Ω is the angular velocity of the earth and ϕ the latitude; v is the northward velocity; A_h is the constant horizontal viscosity coefficient; and ρ_0 is the density.

Although Munk (1950) assumed a constant horizontal viscosity coefficient, in practice the effective horizontal viscosity is expected to increase away from the coast. This is because the viscosity is due to small-scale eddies, and these increase in size as the distance offshore increases.

A similar scale dependence of the viscosity term is found in other boundary layers (Ellison 1956; Landau and Lifshitz 1987). For these, theories in which the viscosity coefficient is proportional to x are known to give good results near the boundary. It is thus of interest to see how a similar scaling affects the structure of an oceanic western boundary current.

We know that the size of the horizontal eddies reaches a maximum a few Rossby radii away from the coastline. We therefore ought to expect the effective viscosity to reach a maximum and either remain constant or decay at farther distances from the coast. It is also not obvious that viscosity should tend to zero at the continental shelf edge because of the strong shears and rough slope topography.

A more complete theory may need to take both of these possibilities into account. However, it is simpler to first work with a viscosity coefficient that is linearly proportional to x. The resulting solutions are of interest in their own right and, as we shall see later, they can be matched to constant viscosity solutions at small and large distances from the coast.

Let us assume, therefore, that A_h is equal to Ax, where A is constant. Equation (1) becomes

$$-fv = -\frac{1}{\rho_0}\frac{\partial p}{\partial x},$$

$$0 = -\frac{1}{\rho_0}\frac{\partial p}{\partial y} + \frac{\partial}{\partial x}\left(Ax\frac{\partial}{\partial x}\right)v. \tag{2}$$

Eliminating the pressure by cross differentiating gives

$$\frac{\partial^2}{\partial x^2}\left(x\frac{\partial}{\partial x}\right)v(x) = k_0^2 v(x), \tag{3}$$

where k_0^2 equals β/A, and β equals $\partial f/\partial y$. Let z equal $k_0 x$. Then,

$$\frac{\partial^2}{\partial z^2}\left(z\frac{\partial}{\partial z}\right)v(z) - v(z) = 0. \tag{4}$$

Power series solution

Equation (4) is a linear differential equation of third order. It will have three independent solutions and the boundary current will be represented by a combination of these, satisfying suitable boundary conditions. Although the equation is of a classic form, it is not discussed in any of the standard texts, for example Abramowitz and Stegan (1965). We therefore have to develop our own analytic solutions.

To obtain the independent solutions, we first try a power series solution (Mathews and Walker 1965) of the form

$$v(z, s) = \sum_{n=0}^{\infty} c_n z^{s+n}. \tag{5}$$

Substituting (5) into (4) and equating the coefficient of z^{s+n}, one finds that, if c_0 equals 1,

$$v(z, s) = z^s + \frac{z^{s+2}}{(s+1)(s+2)^2} + \frac{z^{s+3}}{(s+1)(s+2)^2(s+3)(s+4)^2} + \cdots. \tag{6}$$

Substituting into (4),

$$\frac{\partial^2}{\partial z^2}\left(z\frac{\partial}{\partial z}\right)v(z, s) - v(z, s) = s^2(s-1)z^{s-3}. \tag{7}$$

Thus, $v(z, s)$ is a solution of (4) when s equals 0 and 1. This gives the first two independent solutions. The third is found by taking the derivative of (7) with respect to s. This shows that $\partial v(z, s)/\partial s$ is a solution of (4) when s equals 0.

The three independent solutions are thus

$$v_0(z) = 1 + \frac{z^2}{1\cdot 2^2} + \frac{z^4}{1\cdot 2^2\cdot 3\cdot 4^2} + \cdots, = \sum_{n=0}^{\infty} z^{2n}/[2^n\Gamma(2n+1)\Gamma(n+1)], \tag{8}$$

$$v_1(z) = z + \frac{z^3}{1^2\cdot 2\cdot 3^2} + \frac{z^5}{1^2\cdot 2\cdot 3^2\cdot 4\cdot 5^2} + \cdots, = \sum_{n=0}^{\infty} z^{2n+1}[2^n\Gamma(n+1)/\Gamma(2n+2)^2], \tag{9}$$

and

$$v_2(z) = \ln(z)v_0(z) + \left[\frac{z^2}{1\cdot 2^2}\left(-\frac{1}{1}-\frac{2}{2}\right) + \frac{z^4}{1\cdot 2^2\cdot 3\cdot 4^2}\left(-\frac{1}{1}-\frac{2}{2}-\frac{1}{3}-\frac{2}{4}\right) + \cdots\right]. \tag{10}$$

All three of these functions tend to infinity for large z. For practical use we need solutions that tend to zero at large distances from the coast. A study of the asymptotic properties of the equation (appendix A) shows that there are three independent asymptotic solutions:

$$a_0(z) = z^{-1/3}\exp\left(\frac{3}{2}z^{2/3}\right),$$
$$a_1(z) = z^{-1/3}\exp\left[\left(-\frac{1}{2} + i\frac{\sqrt{3}}{2}\right)\frac{3}{2}z^{2/3}\right],$$
$$a_2(z) = z^{-1/3}\exp\left[\left(-\frac{1}{2} - i\frac{\sqrt{3}}{2}\right)\frac{3}{2}z^{2/3}\right]. \tag{11}$$

Note the similarities with the solutions of Munk's equation (28). Of the three asymptotic solutions, only a_0 increases exponentially at large z. Thus, as v_0, v_1, and v_2 correspond asymptotically to linear combinations of a_0, a_1, and a_2; all are dominated at large z by their a_0 component and have similar behavior. As a result (see appendix B),

$$\lim_{z\to\infty}\left(\frac{v_1(z)}{v_0(z)}\right) = \left(\frac{\pi}{2}\right)^{1/2},$$
$$\lim_{z\to\infty}\left(\frac{v_2(z)}{v_0(z)}\right) = \frac{1}{2}\ln(2) - \frac{3}{2}\gamma \approx -0.5192499\cdots, \tag{12}$$

where γ is Euler's constant (0.577 215 664 . . .).

It is thus convenient to define the independent solutions $W_1(z)$, $W_2(z)$, and $W_3(z)$ as

$$W_0(z) = \left(\frac{\pi}{2}\right)^{1/2} v_0(z) + v_1(z), \tag{13}$$

$$W_1(z) = \left(\frac{\pi}{2}\right)^{1/2} v_0(z) - v_1(z), \tag{14}$$

$$W_2(z) = \left(\frac{2}{\pi}\right)^{1/2}\left[v_2(z) + \left(\frac{3}{2}\gamma - \frac{1}{2}\ln(2)\right)v_0(z)\right]. \tag{15}$$

These are plotted in Fig. 2. Using the relationship [Abramowitz and Stegan (1965), Eq. (6.1.18)],

$$\Gamma(2n) = (2\pi)^{-1/2}2^{2n-1/2}\Gamma(n)\Gamma(n+\tfrac{1}{2}),$$

one can also show that

$$W_0(z) = \left(\frac{\pi}{2}\right)^{1/2}\sum_{n=0}^{\infty}\frac{z^n}{[2^{n/2}\Gamma(n+1)\Gamma(n/2+1)]} \tag{16}$$

and that

$$W_1(z) = W_0(-z). \tag{17}$$

For large z,

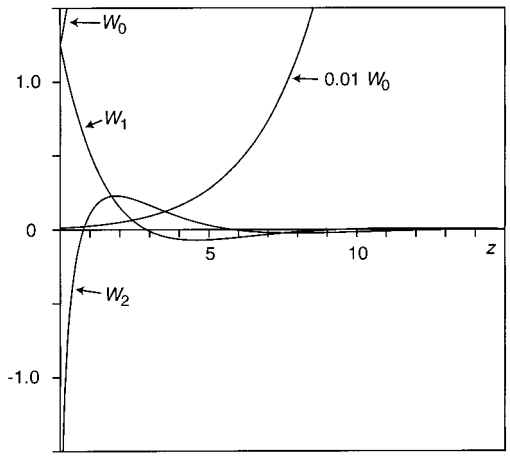

FIG. 2. The functions $W_0(z)$, $W_1(z)$, and $W_2(z)$.

$$\lim_{z\to\infty} W_0(z) = \left(\frac{1}{3}\right)^{1/2} a_0(z),$$

$$\lim_{z\to\infty} W_1(z) = \left(\frac{1}{3}\right)^{1/2} e^{-i\pi/3} a_1(z) + \text{c.c.},$$

$$\lim_{z\to\infty} W_2(z) = \left(\frac{1}{3}\right)^{1/2} e^{-i5\pi/6} a_1(z) + \text{c.c.} \qquad (18)$$

Here W_0 increases exponentially at large z, and W_1 and W_2 are the exponentially decaying solutions that we require.

The other limit of interest is near the origin:

$$\lim_{x\to 0} W_0(z) = \left(\frac{\pi}{2}\right)^{1/2} + z + O(z^2),$$

$$\lim_{x\to 0} W_1(z) = \left(\frac{\pi}{2}\right)^{1/2} - z + O(z^2),$$

$$\lim_{x\to 0} W_2(z) = \left(\frac{2}{\pi}\right)^{1/2} \left(\ln(z) + \frac{3}{2}\gamma - \frac{1}{2}\ln(2)\right) + O(z^2). \qquad (19)$$

In Eq. (18), the asymptotic limit for $W_0(z)$ was obtained analytically (appendix B). The limits for $W_1(z)$ and $W_2(z)$ were obtained numerically, using a computer to estimate the combinations of a_1 and a_2 that fit W_1 and W_2 at large z. The coefficient values were identified as being close to the analytic values shown, so a further check was carried out using Fortran real*16 arithmetic to reduce the rounding errors when calculating W_1 and W_2 at large z. This confirmed that the analytic values are correct to at least seven decimal places.

In the same way and to the same accuracy we also have

$$\int_0^\infty W_1(z)\, dz = 1,$$

$$\int_0^\infty W_2(z)\, dz = 0. \qquad (20)$$

Thus $W_1(z)$ is well behaved, but $W_2(z)$ is unusual, having a logarithmic singularity near the coast and contributing nothing to the integrated velocity (i.e., the total transport of the current).

If the lower limit on z is ε, where ε is small and positive, then from (19) and (20)

$$\int_\varepsilon^\infty W_1(z)\, dz = 1 - \left(\frac{\pi}{2}\right)^{1/2} \varepsilon + O(\varepsilon^2),$$

$$\int_\varepsilon^\infty W_2(z)\, dz = -\left(\frac{2}{\pi}\right)^{1/2} \varepsilon \left(\ln\varepsilon - 1 + \frac{3}{2}\gamma - \frac{1}{2}\ln(2)\right) + O(\varepsilon^2). \qquad (21)$$

3. The western boundary current problem

The boundary conditions for the western boundary current problem are that the velocity should tend to zero at large distances from the coast, that the total transport should be some fixed number, and that the velocity should tend to zero at the coast.

Because the velocity field is expected to behave logarithmically near the coastline, giving a singularity at the coast itself, the coastal boundary condition is actually more complex. The standard solution is to set the velocity to zero at a distance ε' from the coastline. The roughness length ε' is chosen to represent the small roughness elements near to the coast.

We will continue using the nondimensional form of the equations, so let ε, equal to $k_0\varepsilon'$, be the nondimensional roughness length. The boundary condition at large distances from the coast means that the general solution to (4) is of the form

$$v(z) = AW_1(z) + BW_2(z). \qquad (22)$$

Near the origin, the boundary condition gives

$$AW_1(\varepsilon) + BW_2(\varepsilon) = 0. \qquad (23)$$

For unit transport we require

$$1 = \int_\varepsilon^\infty v(z)\, dz$$

$$= A\int_\varepsilon^\infty W_1(z)\, dz + B\int_\varepsilon^\infty W_2(z)\, dz$$

$$= A\left(1 - \int_0^\varepsilon W_1(z)\, dz\right) - B\int_0^\varepsilon W_2(z)\, dz. \qquad (24)$$

The integrals are evaluated by substituting the power series expansions of W_1 and W_2 and reversing the order of integration and summation. Equations (23) and (24)

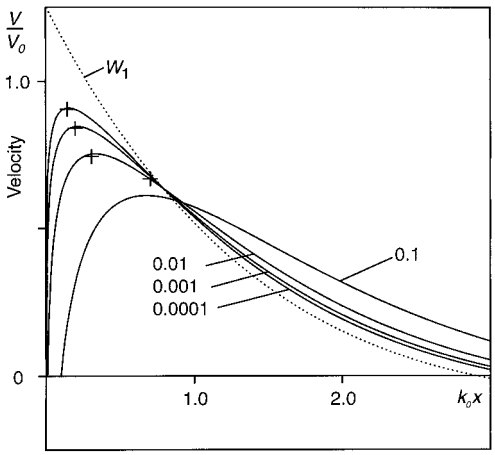

FIG. 3. The alongshore velocity plotted for different values of ε. The dotted line is the function W_1. The crosses indicate the position of the current maximum estimated from (26).

can then be solved for A and B. Figure 3 shows the resulting velocity field for a series of values of ε.

The figure uses nondimensional units for the axes. If A equals 0.1 m s^{-1}, then at 30°S, where β equals 1.14 $\times$ 10^{-11}, the horizontal scale length k_0^{-1} is 93 km. At this distance from the coast the viscosity is 9.3 $\times$ 10^3 m^2 s^{-1}. The velocity scale V_0 equals $(k_0 T/D)$, where T is the total transport in the boundary current and D is its depth. If T equals 20 Sv (Sv $\equiv$ 10^6 m^3 s^{-1}) and D is 1 km, then V_0 equals 21 cm s^{-1}.

Near the coast the solutions are dominated by the logarithmic boundary layer. However, the velocity soon peaks and drops away, giving the western boundary current. Offshore, the velocity field oscillates in sign and decays rapidly, the wavelength of the oscillations increasing away from the coast.

The results show that the roughness length affects the magnitude and position of the current maximum but that it has little effect on the total width of the boundary current. The latter is approximately equal to $3k_0^{-1}$.

When ε is small,

$$A = 1 + O(\varepsilon)$$

$$B = \left(\frac{\pi}{2}\right) \Big/ \left(\frac{1}{2}\ln(2) - \frac{3}{2}\gamma - \ln(\varepsilon)\right) + O(\varepsilon). \quad (25)$$

Substituting (25) and (19) in (22), the current maximum $v_{\max}$ is found at a distance $x_{\max}$ from the coast, where

$$k_0 x_{\max} = B\left(\frac{2}{\pi}\right)^{1/2} + O(\varepsilon),$$

$$v_{\max} = \left(\frac{\pi}{2}\right)^{1/2} + \left(\ln(k_0 x_{\max}) + \frac{3}{2}\gamma - \frac{1}{2}\ln(2) - 1\right) + O(\varepsilon). \quad (26)$$

These values are plotted as small crosses in Fig. 3. The agreement with the exact solution is good for the cases where ε is less than 0.1.

4. The Munk and Stommel solutions

It is of interest to compare these solutions with those obtained by Munk, who assumed A_h was constant, and by Stommel, who used bottom friction.

If A_h is constant, then instead of (3) we obtain

$$\frac{\partial^3}{\partial x^3} v(x) = k_m^3 v(x), \quad (27)$$

where k_m^3 equals β/A_h. The three independent solutions are

$$v_{m1}(x) = k_m \frac{2}{\sqrt{3}} \exp\left(-\frac{1}{2}k_m x\right) \sin\left(\frac{\sqrt{3}}{2}k_m x\right),$$

$$v_{m2}(x) = k_m 2 \exp\left(-\frac{1}{2}k_m x\right) \cos\left(\frac{\sqrt{3}}{2}k_m x\right),$$

$$v_{m3}(x) = k_m \exp\left(+\frac{1}{2}k_m x\right). \quad (28)$$

The solution v_{m1}, which is zero at the coast, tends to zero far from the coast, and has unit transport per unit depth, is the solution used by Munk (1950) to describe western boundary currents.

Stommel (1948) assumed that the north–south pressure gradient was balanced by bottom friction. Equations (1) then become

$$-fv = -\frac{1}{\rho_0}\frac{\partial p}{\partial x},$$

$$0 = -\frac{1}{\rho_0}\frac{\partial p}{\partial y} - \frac{\kappa}{H}v, \quad (29)$$

where H is the depth of the ocean and κ is the coefficient of bottom friction. Equation (3) now becomes

$$\frac{\partial}{\partial x} v(x) = -k_s v(x), \quad (30)$$

where k_s equals $\beta H/\kappa$.

The solution with unit transport per unit depth is

$$v_s(x) = k_s \exp(-k_s x). \quad (31)$$

The two solutions $v_{m1}(x)$ and $v_s(x)$ are plotted in Fig. 4 together with the solutions of (3) obtained earlier. For the comparison both k_m and k_s are set to unity. For the Munk solution, this is equivalent to using a viscosity coefficient equal to that at the point where $k_0 x$ equals one in the linearly varying case (i.e., near the center of the boundary current). For the Stommel solution, the choice gives unit current at the coastline.

In many ways the solutions are remarkably similar: for example, the first zero crossings of the Munk and variable viscosity solutions all occur in the same region

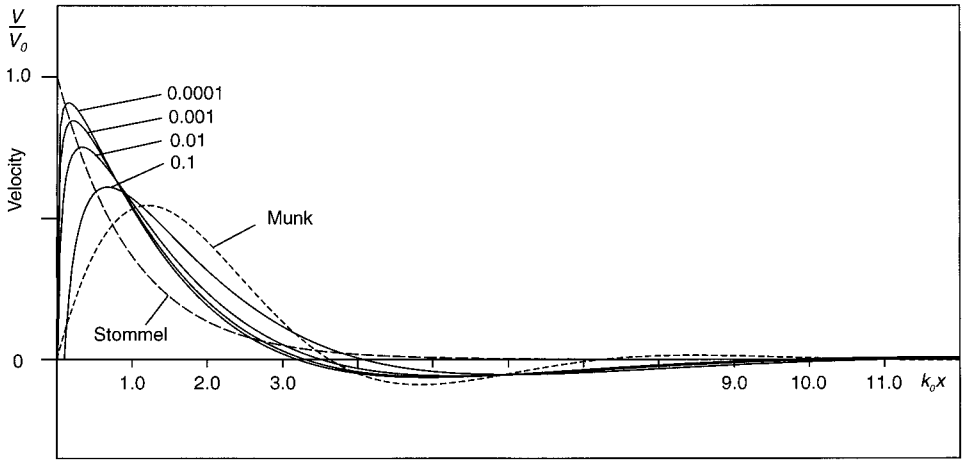

FIG. 4. The alongshore velocity with different values of ε compared with the Munk and Stommel solutions.

with k_0x between 3 and 5. The Stommel solution has no zero crossing, having no countercurrent, but by k_0x equals 5 its amplitude is negligible.

The main differences are in the details of the current maxima. The maximum for the Stommel solution is at the coast and for the Munk solution it is relatively far offshore. Compared with the variable viscosity solutions, the latter arises because the Munk equation has a higher horizontal viscosity near the coast. Offshore, the Munk solution has a narrower return flow region, a result of its lower viscosity.

Overall, the main effect of using a scale-dependent viscosity coefficient is the generation of a logarithmic boundary layer near the coast and the resulting movement of the current maximum toward the coastline. Offshore it produces a broader countercurrent region, a direct result of the higher horizontal viscosity in the region.

5. Force and shear stress

Consider the general form of Eqs. (1) and (2), where the alongshore pressure gradient is balanced by the offshore gradient of a shear stress $S(x)$:

$$-\rho_0 f v = -\frac{\partial p}{\partial x},$$

$$0 = -\frac{\partial p}{\partial y} + \frac{\partial}{\partial x}S(x). \tag{32}$$

In physical terms, $S(x)$ represents the onshore or offshore transport of alongshore momentum. If it depends on a local eddy viscosity $A(x)$ and the local velocity gradient, then

$$S(x) = \rho_0 A(x)\frac{\partial}{\partial x}v(x). \tag{33}$$

However, the general results derived in this section are not dependent on this equation and will hold whatever physical mechanism is responsible for the shear stress.

Eliminating the pressure from (32)

$$\frac{\partial^2}{\partial x^2}S(x) = \rho_0 \beta v(x). \tag{34}$$

Let the transport offshore of x be denoted by $T(x)$. Then,

$$T(x) = \int_x^\infty v(x')\, \partial x'. \tag{35}$$

From (34),

$$T(x) = \frac{1}{\rho_0\beta}\int_x^\infty \left(\frac{\partial^2}{\partial x'^2}S(x')\right) \partial x'$$

$$= \frac{1}{\rho_0\beta}\left[\frac{\partial}{\partial x'}S(x')\right]_x^\infty$$

$$= \frac{1}{\rho_0\beta}[F(\infty) - F(x)], \tag{36}$$

where $F(x)$ is the force per unit volume acting on the fluid. The solution decays offshore, so F is zero at infinity. Thus,

$$F(x) = -\rho_0\beta T(x). \tag{37}$$

At the coast,

$$F(0) = -\rho_0\beta T(0). \tag{38}$$

Thus, the force acting on the water adjacent to the coast depends only on the total transport and the value of β and is independent of the detailed structure of the current or the form of the viscosity $A(x)$. From (32), $F(0)$ is also equal to the alongshore pressure gradient.

The force $F(x)$ is plotted in Fig. 5 for different values

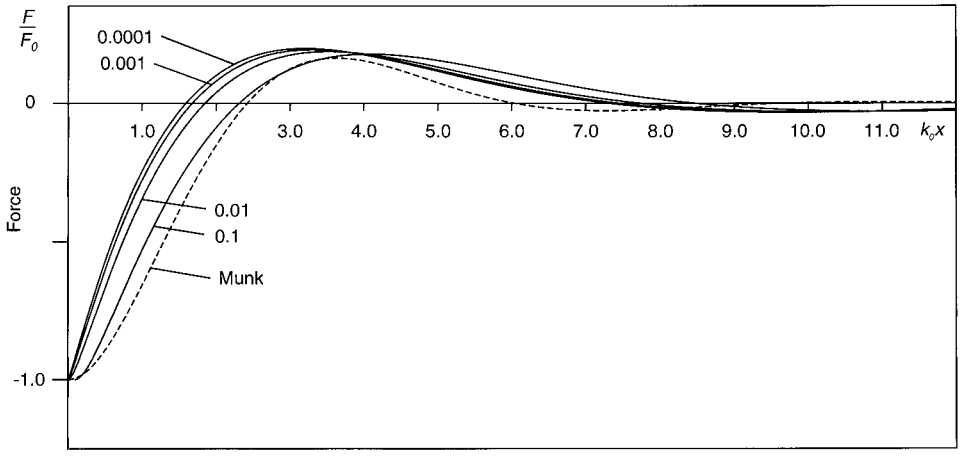

FIG. 5. The alongshore force $F(x)$ for different values of ε compared with the Munk solution.

of ε and for the Munk solution. The functions were evaluated by substituting the power series expansions of v and reversing the order of differentiation and summation. In the figure, the scale force F_0 equals $(\rho_0 \beta T/D)$. With the values quoted earlier (20 Sv in the top 1000 m at 30°S), F_0 equals 2.3×10^{-4} N m^{-3}.

At the coast the solutions all tend to the same value because they have the same transport. Far offshore the Munk solution decays most rapidly, the new solutions again showing the effect of the much higher viscosity that produces a slower offshore decay.

The shear stress $S(x)$ can also be written in the form

$$\begin{aligned} S(x) &= -\int_x^\infty F(x')\,dx' \\ &= \rho_0\beta \int_x^\infty T(x')\,dx' \\ &= \rho_0\beta \int_x^\infty dx' \int_{x'}^\infty v(x'')\,dx'' \\ &= \rho_0\beta \int_x^\infty (x' - x)v(x')\,dx'. \end{aligned} \tag{39}$$

Thus,

$$\begin{aligned} S(0) &= \rho_0\beta \int_0^\infty T(x)\,dx \\ &= \rho_0\beta \int_0^\infty xv(x)\,dx. \end{aligned} \tag{40}$$

This shows that the shear stress at the coast depends on the integral of the transport or the first moment of the current field. For a simple boundary current without countercurrents, the shear stress at the coast can never be zero or negative, but it is least when the current is in the form of a jet close against the coast. In the more usual case, when there is a series of currents and countercurrents, the offshore countercurrents reduce the stress on the coastline and, in principal, can make it negative.

The distribution of shear stress $S(x)$ for the cases considered above is plotted in Fig. 6. The unit of stress S_0 equals $(\rho_0 A k_0 T/D)$. With the values quoted earlier, S_0 equals 21 N m^{-2}.

At the coast the broad Munk solution produces the greatest stress. For the other cases, the stress is reduced as ε becomes smaller and the peak of the main current moves toward the coast. Offshore the countercurrent region has a large effect on the shear stress but the total effect of the offshore currents, as measured by the minimum value of the shear stress, is only weakly affected by changes in ε.

6. Application to the Agulhas Current data

We consider first the case where the viscosity increases linearly away from the boundary. For the data taken at a depth of 237 m, the boundary is assumed to be the point 8.6 km from the coast where the continental slope has this depth. As with (22), we ignore any small Sverdrup transport at large distances from the coast and assume that the velocity field has the form

$$v(x) = AW_1\left(\frac{x}{x_0}\right) + BW_2\left(\frac{x}{x_0}\right). \tag{41}$$

The solution has three free parameters, the horizontal scale length x_w (equal to k_0^{-1}), the roughness length ε, and the current transport (24). These were estimated by minimizing the variance σ^2 between the analytic solution (41) and the Agulhas Current data,

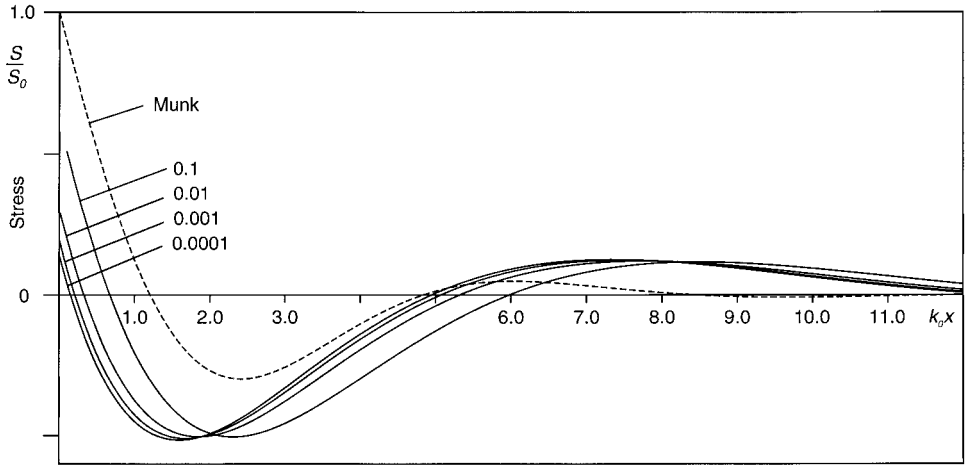

FIG. 6. The viscous shear stress $S(x)$ for different values of ε compared with the Munk solution.

$$\sigma^2 = \sum_i (v_i - v(x_i))^2, \tag{42}$$

where v_i is the velocity data at distance x_i from the coast. The problem is a nonlinear one in terms of x_w and ε, but if these are fixed, it transforms into a linear equation for the total transport. NAG routine E04FDF (NAG 1993) was used to estimate the best-fit values of x_{m1} and ε, the transport being calculated from the linear equation during each iteration.

The resulting best fit is shown in Fig. 7. Parameter values and the residual variance are given in Table 1 (case L). At 31.5°S and with the coast at an angle of 40°, a scale length x_w of 64.57 km corresponds to the coefficient A having a value of 0.063 m s^{-1}.

Diffusion is an integral effect due to all unresolved time-dependent motions, but it sometimes helps to consider it in terms of some dominant eddy field. In the present case such eddies have a velocity of order 0.06 m s^{-1} and a horizontal scale comparable to the distance from the coast. The estimated velocity is about 5% of the maximum velocity measured in the core of the Agulhas Current and is not unreasonable for transient motions.

Although the viscosity is low near the boundary, in the core of the current 17 km from the boundary it has risen to 1383 m^2 s^{-1}. At 100 km, the viscosity is 8139 m^2 s^{-1}. This continued increase offshore is almost certainly unphysical. However, the current shear at large distances is small, so if the viscosity levels off, or becomes smaller, the effect on the velocity profile should be small.

Figure 7 and the table of variances show that a linearly increasing viscosity gives a reasonably good fit to the Agulhas Current data. Although the new solution has only one more parameter than the Munk solution, the position and magnitude of the peak of the current are fitted well, as is the decaying tail. The residual variance also drops from 24% with the two parameter Munk

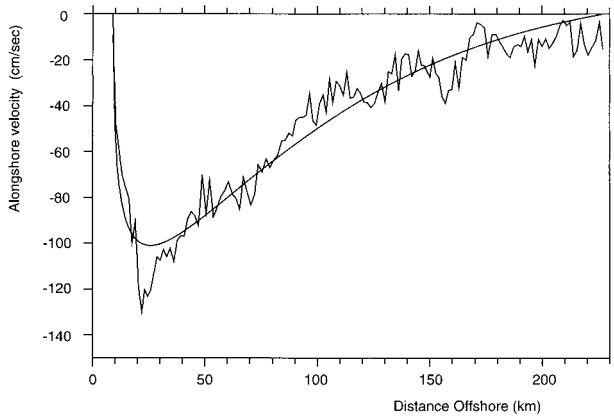

FIG. 7. The best-fit solution to the data obtained with a linearly varying viscosity. The best-fit parameters are tabulated as model L in Table 1.

TABLE 1. Variance of the raw data and the best-fit residual variance for each of the models together with the model parameters. In the model names, C and L refer to constant and linearly varying viscosity regions and are ordered starting from the shelf edge. Here x_1 and x_2 are the distances of the inner and outer boundaries between the regions from the shelf edge; x_{m1} and x_w are the scale lengths for the inner and linearly varying region, respectively. For model L, when there is no coastal constant viscosity region, x_1 is the roughness length.

Model	Residual variance (cm^2 s^{-2})	Variance explained (%)	x_{m1} (km)	x_1 (km)	x_w (km)	x_2 (km)
Data	449 080.3					
C	107 611.2	76.04	38.35			
L	12 055.7	97.32		0.23	64.57	
L-C	12 056.6	97.32		0.22	64.65	581.8
C-L	8104.6	98.20	18.99	18.61	81.74	
C-L-C	8104.6	98.20	18.99	18.62	81.74	876.1

solution to 2.3% with the new solution. This appears to be statistically significant, but unfortunately an F test cannot be used because the underlying models are nonlinear. (If it was valid, then the improvement would be significant at the 99% level.)

The major remaining discrepancies between the solution and the data are the inshore current shear, which is too large, the shape of the current maximum, which is too wide, and the offshore zero crossing, which is not present in the data. The first two indicate that the viscosity may be too small near the coast and too large near the peak of the current. The offshore zero crossing is more difficult and is discussed later.

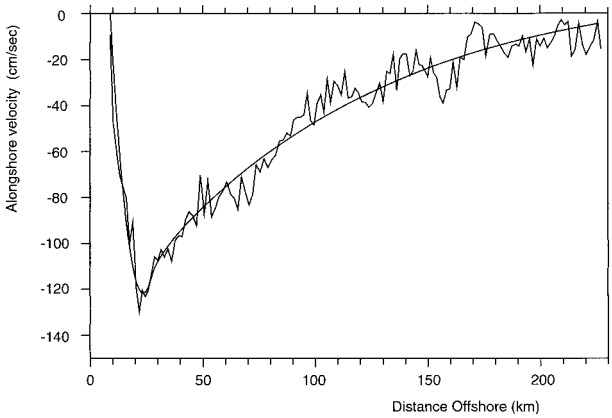

FIG. 8. The best-fit solution to the data with a coastal constant viscosity layer matched to an offshore linearly varying viscosity. The best-fit parameters are tabulated as model C–L in Table 1.

Mixed solutions

As we now have analytic solutions for both the constant viscosity and linearly varying viscosity problems, it is possible to consider more complex cases. Three will be considered. The first, denoted C-L, has an inshore region where the viscosity is constant and an offshore region where it is linearly varying. The viscosities are equal at the matching point. The second case, L-C, has an inshore linearly varying region matched to an offshore constant viscosity region. The final case, C-L-C, has both inshore and offshore constant viscosity regions matched to an intermediate linearly varying region.

For the first case, C-L, the offshore velocity is given by (41) and the inshore velocity is a linear combination of the three Munk functions given by (28). If the boundary between the two regions is at x equal to x_1, then the boundary conditions are obtained by integrating (32) between $x_1 - \varepsilon$ and $x_1 + \varepsilon$, where ε is positive and infinitesimally small:

$$\frac{\partial}{\partial x}\left(A(x)\frac{\partial}{\partial x}\right)v(x)\bigg|_{x_1-\varepsilon} = \frac{\partial}{\partial x}\left(A(x)\frac{\partial}{\partial x}\right)v(x)\bigg|_{x_1+\varepsilon},$$

$$\left(A(x)\frac{\partial}{\partial x}\right)v(x)\bigg|_{x_1-\varepsilon} = \left(A(x)\frac{\partial}{\partial x}\right)v(x)\bigg|_{x_1+\varepsilon},$$

$$v(x)|_{x_1-\varepsilon} = v(x)|_{x_1+\varepsilon}. \tag{43}$$

In physical terms, these equations require the force, shear stress, and velocity all to be continuous across the boundary.

For the second case, L-C, the inshore velocity is a linear combination of the three W functions (13), and the offshore velocity is a linear combination of the two decaying Munk solutions, v_{m1} and v_{m2} (28). The final case, C-L-C, adds three more Munk functions to describe the inner constant viscosity layer.

In each of the cases, the free parameters were varied as before to give the best fit as measured by Eq. (42). The resulting parameters and residual variances are given in Table 1.

In case C-L, the addition of the inner constant viscosity layer reduces the residual variance by a third. (With a linear system such an improvement would be significant at the 99% level.) The improved solution is illustrated in Fig. 8. Note that the inshore constant viscosity layer extends beyond the peak of the current. The slight kink in the velocity field 30 km from the coast is associated with the change of the offshore gradient of viscosity at the matching point (43).

In this case, the values of x_w and x_{m1} give a value of A equal to 0.1 m s^{-1} and a value of the viscosity coefficient A_h in the inner constant viscosity layer equal to 102 m^2 s^{-1}. The value of x_1 is also roughly equal to the position of the Agulhas Current maximum. If, as before, we assume that the viscosity is due to an eddy field with velocities of order 0.1 m s^{-1}, then the eddy field inshore of the current maximum has a scale of order 1 km. The results imply that the underlying turbulent field is relatively constant inshore of the current maximum and that it increases in scale offshore of this maximum.

In the two cases, L-C and C-L-C, the addition of the offshore constant viscosity layer does not improve the solution significantly. (The minimization algorithm actually tries to move the boundaries as far offshore as possible, the resulting velocity profiles being similar to Figs. 7 and 8, respectively.) These results are surprising, as in practice one would expect the amount of energy in the eddy field to reach a maximum and decay at distances beyond a few Rossby radii from the coastline and maximum current.

The failure to provide an offshore upper bound on the viscosity may be associated with the problem of the zero crossing. If we consider the case of arbitrary viscosity, then from (39), if the shear stress falls to zero anywhere, the offshore velocity must have zero first moment. A corollary of this result is that, if there is no zero crossing as appears to be true in the Agulhas data,

the stress must have the same sign everywhere. In this case, the shear stress cannot be a function of the local current shear. Instead it must still be responding to the coastal boundary condition even at distances far offshore beyond the peak in the Agulhas Current.

The alternatives are that the Bryden (1995) data is atypical or that additional physics is involved. The latter might be a result of offshore flow at large distances from the coast. It could also be associated with the relatively tight recirculation gyre and the alongshore acceleration of the Agulhas Current (Pierce 1977; Stramma and Lutjeharms 1997). Time-dependent processes may also be involved.

7. Conclusions

We have investigated whether the observed velocity structure of the Agulhas Current can be understood in terms of geostrophic balance and simple ideas of eddy viscosity. The standard Munk western boundary current was found to provide a poor fit to the data, explaining only 76% of the variance. This arose primarily because the solution cannot reproduce both the large shear near the coast and the slow decay of the current offshore. It was therefore decided to develop an analytic solution for the case where the viscosity varies linearly with distance from the coast.

The investigation showed that the resulting boundary current has a logarithmic layer near the coast and a nearshore current maximum. Offshore the current decays and oscillates, giving a series of currents and countercurrents similar to the Munk solution but with the wavelength increasing offshore.

The structure of the force and shear stress fields have also been investigated. For an arbitrary horizontal viscosity, the viscous force acting on water adjacent to the coast is proportional to the total transport, that is, the integral of the velocity field. Also the stress on the coastline is equal to the first moment of the velocity field. For the present series of solutions this means that the stress on the coast is smallest when the boundary roughness ε is small and the boundary current is narrowest.

The new analytic solution has been used to fit the data collected from the Agulhas Current. It fitted well, except near the continental shelf edge where the shear was too large, and was found to explain 97.3% of the variance. The addition of a constant viscosity inshore layer produced a further significant improvement, reducing the shear near the coast and explaining 98.2% of the total variance. Adding a second constant viscosity region far from the coast, to represent an offshore limit to the viscosity, did not improve the fit significantly.

Acknowledgments. I wish to acknowledge the role of Dr. H. Bryden, who made the Agulhas Current measurements, suggested the problem, and provided encouragement during its solution. Thanks also to the referees for their testing comments and to Mr. P. Challenor for discussions on the statistical theory.

APPENDIX A

Asymptotic Series Solution

The equivalent second-order form of (4) has solutions involving Hankel functions (Ellison 1956; Abramowitz and Stegan 1965). These have the asymptotic form

$$\varphi(z) \approx z^s \exp(i\alpha z), \tag{A1}$$

where α is complex. Various tests based on this form show that the function $v_0(z)$ behaves as $\exp(\alpha z^{2/3})$. With this in mind, we try the substitution ζ equal to $z^{2/3}$. Then (4) becomes

$$\frac{\partial^3 v}{\partial \zeta^3} + \frac{3}{2\zeta}\frac{\partial^2 v}{\partial \zeta^2} - \frac{1}{2\zeta^2}\frac{\partial v}{\partial \zeta} - \left(\frac{3}{2}\right)^2 v = 0. \tag{A2}$$

Try the asymptotic series

$$v(\zeta) = \exp(\alpha\zeta)\sum_{n=0}^{\infty} c_n \zeta^{s-n}. \tag{A3}$$

Substituting in (A2), setting c_0 to unity, and equating coefficients of ζ^{s+n} gives

$$\begin{aligned} s &= -1/2, \\ \alpha &= \left(\frac{3}{2}\right)1^{1/3}, \\ c_1 &= 1/(12\alpha), \\ c_n &= \frac{c_{n-1}(3(1/2-n)^2 - 1/2) + c_{n-2}(3/2-n)((1/2-n)(1-n) - 1/2)}{3n\alpha^2}. \end{aligned} \tag{A4}$$

Here $1^{1/3}$ means the three complex cube roots of 1, that is, $+1$ and $(-1 \pm i(3)^{1/2})/2$. Equation (11) contains the leading term of the three resulting series written as a function of z.

APPENDIX B

Power Series Asymptotic Limits

Equation (6) can be rewritten in terms of Gamma functions as

$$\upsilon(z, s) = \sum_{n=0}^{\infty} z^{2n+s} \frac{\Gamma(s+1)\Gamma(s/2+1)}{\Gamma(2n+s+1)\Gamma(n+s/2+1)2^n}. \quad \text{(B1)}$$

Using Stirling's formula,

$$\lim_{z\to\infty} \Gamma(z) = e^{-z} z^{z-1/2} (2\pi)^{1/2}, \quad \text{(B2)}$$

and

$$\lim_{b/a\to\infty} (a+b)^a = a^a e^b, \quad \text{(B3)}$$

one finds that for large z,

$$\upsilon(z,s) \approx \sum_{n=0}^{\infty} z^{2n+s} \frac{\Gamma(s+1)\Gamma(s/2+1)3^{3n+(3/2)s+1}}{(2\pi)^{1/2}2^{3n+s+1/2}\Gamma\left(3n+\frac{3}{2}s+\frac{3}{2}\right)}. \quad \text{(B4)}$$

Let ζ equal $z^{2/3}$. Then,

$$\begin{aligned}
\upsilon(z, s) &\approx \frac{\Gamma(s+1)\Gamma(s/2+1)3^{(3/2)s+1}}{(2\pi)^{1/2}2^{s+1/2}} \\
&\quad \times \sum_{n=0}^{\infty} \zeta^{3n+(3/2)s} \left(\frac{3}{2}\right)^{3n} \Bigg/ \Gamma\left(3n+\frac{3}{2}s+\frac{3}{2}\right), \\
&\approx \frac{\Gamma(s+1)\Gamma(s/2+1)3^{1/2}2^{s/2}}{(2\pi)^{1/2}} \\
&\quad \times \zeta^{-1/2} \sum_{n=0}^{\infty} \left(\frac{3}{2}\zeta\right)^{3n+(3/2)s+1/2} \Bigg/ \Gamma\left(3n+\frac{3}{2}s+\frac{3}{2}\right), \\
&\approx \frac{\Gamma(s+1)\Gamma(s/2+1)3^{1/2}2^{s/2}}{(2\pi)^{1/2}} \zeta^{-1/2} \frac{1}{3} \exp\left(\frac{3}{2}\zeta\right).
\end{aligned} \quad \text{(B5)}$$

Thus, for large z,

$$\upsilon(z,s) = \frac{\Gamma(s+1)\Gamma(s/2+1)2^{s/2}}{(6\pi)^{1/2}} z^{-1/3} \exp\left(\frac{3}{2}z^{2/3}\right). \quad \text{(B6)}$$

The asymptotic forms of υ_0 and υ_1 are obtained with s equal to 0 and 1, respectively,

$$\begin{aligned}
\upsilon_0(z) &\approx \left(\frac{1}{6\pi}\right)^{1/2} z^{-1/3} \exp\left(\frac{3}{2}z^{2/3}\right), \\
\upsilon_1(z) &\approx \left(\frac{1}{12}\right)^{1/2} z^{-1/3} \exp\left(\frac{3}{2}z^{2/3}\right).
\end{aligned} \quad \text{(B7)}$$

The asymptotic form of υ_2 is obtained from the derivative of (B6) with respect to s:

$$\begin{aligned}
\frac{\partial}{\partial s}\upsilon(z,s) &\approx \frac{1}{(6\pi)^{1/2}} z^{-1/3} \exp\left(\frac{3}{2}z^{2/3}\right) \\
&\quad \times \frac{\partial}{\partial s}\left(\Gamma(s+1)\Gamma(s/2+1)2^{s/2}\right), \\
&\approx \frac{1}{(6\pi)^{1/2}} z^{-1/3} \exp\left(\frac{3}{2}z^{2/3}\right)\Gamma(s+1)\Gamma(s/2+1)2^{s/2} \\
&\quad \times \left(\psi(s+1) + \frac{1}{2}\psi\left(\frac{s}{2}+1\right) + \frac{\ln(2)}{2}\right),
\end{aligned} \quad \text{(B8)}$$

where Ψ is the Psi (or Digamma) function. Thus, when s equals 0,

$$\upsilon_2(z) \approx \frac{1}{(6\pi)^{1/2}} z^{-1/3} \exp\left(\frac{3}{2}z^{2/3}\right)\left(\frac{\ln(2)}{2} - \frac{3}{2}\gamma\right). \quad \text{(B9)}$$

REFERENCES

Abramowitz, M., and I. A. Stegan, 1965: *Handbook of Mathematical Functions.* Dover, 1046 pp.

Beal, L. M., and H. L. Bryden, 1997: Observations of an Agulhas undercurrent. *Deep-Sea Res.*, **44** (9/10), 1715–1724.

Bryden, H. L., 1995: RRS *''Discovery''* Cruise 214, 26 Feb–09 Mar 1995: Agulhas Current Experiment. Cruise Report 249, Institute of Oceanographic Sciences Deacon Laboratory, 85 pp.

Ellison, T. H., 1956: Atmospheric turbulence. *Surveys in Mechanics*, G. K. Batchelor and R. M. Davies, Eds., Cambridge University Press, 400–430.

Grundlingh, M. L., 1983: On the course of the Agulhas Current. *S. Afr. Geogr. J.*, **65,** 49–57.

Landau, L. D., and E. M. Lifshitz, 1987: *Fluid Mechanics.* 2d ed. Butterworth-Heinemann, 539 pp.

MacCready, P., and P. B. Rhines, 1993: Slippery boundary layers on a slope. *J. Phys. Oceanogr.*, **23,** 5–22.

Mathews, J., and R. L. Walker, 1965: *Mathematical Methods of Physics.* W. A. Benjamin Inc., 475 pp.

Munk, W. H., 1950: On the wind-driven ocean circulation. *J. Meteor.*, **7**(2), 79–93.

NAG, 1993: *The NAG Fortran Manual, Mark 16.* Vol. 4. NAG, 453 pp. [Available from Numerical Algorithms Group (NAG) Ltd, Jordon Hill Road, Oxford OX2 8DR, United Kingdom.].

Pierce, A. F., 1977: Features of the upper 500 m of the Agulhas Current. *J. Mar. Res.*, **35,** 731–753.

Stommel, H., 1948: The westward intensification of wind-driven ocean currents. *Trans. Amer. Geophys. Union,* **29**(2), 202–206.

Stramma, L., and J. R. E. Lutjeharms, 1997: The flow field of the subtropical gyre of the South Indian Ocean. *J. Geophys. Res.*, **102,** 5513–5530.

Toole, J. M., and B. A. Warren, 1993: A hydrographic section across the subtropical South Indian Ocean. *Deep-Sea Res.*, **40,** 1973–2019.